A Sea Surface Height Perspective on El Niño Diversity, Ocean Energetics, and Energy Damping Rates

Jian Shi, Alexey V. Fedorov, Shineng Hu

Geophysical Research Letters

RESEARCH LETTER
10.1029/2019GL086742

A Sea Surface Height Perspective on El Niño Diversity, Ocean Energetics, and Energy Damping Rates

Jian Shi[1,2], **Alexey V. Fedorov**[3,4], **and Shineng Hu**[5]

[1]Key Laboratory of Physical Oceanography, Institute for Advanced Ocean Study, Ocean University of China and Qingdao National Laboratory for Marine Science and Technology, Qingdao, China, [2]College of Oceanic and Atmospheric Sciences, Ocean University of China, Qingdao, China, [3]Department of Earth and Planetary Sciences, Yale University, New Haven, CT, USA, [4]LOCEAN/IPSL, Sorbonne University, Paris, France, [5]Lamont-Doherty Earth Observatory, Columbia University, Palisades, NY, USA

Key Points:
- A sea surface height index (SSHI) is introduced as a linear component of anomalous SSH squared and averaged over the tropical Pacific
- SSHI records thermocline variations, approximates ocean energetics in the tropical Pacific, and helps distinguish different El Niño types
- SSHI gives an estimate of the damping timescale of available potential energy in the tropical Pacific ocean of approximately 1.7 years

Supporting Information:
- Supporting Information S1

Correspondence to:
J. Shi, and A. V. Fedorov,
shijian@ouc.edu.cn
alexey.fedorov@yale.edu

Citation:
Shi, J., Fedorov, A. V., & Hu, S. (2020). A sea surface height perspective on El Niño diversity, ocean energetics, and energy damping rates. *Geophysical Research Letters*, *47*, e2019GL086742. https://doi.org/10.1029/2019GL086742

Received 19 DEC 2019
Accepted 23 MAR 2020
Accepted article online 28 MAR 2020

Abstract Ocean energetics is a useful framework for understanding El Niño–Southern Oscillation; however, its key element, available potential energy (APE), requires accurate ocean subsurface data that are hard to measure. Here, we describe a sea surface height-based index, SSHI, that accurately captures APE variations and can be easily computed from satellite observations. Using SSHI, we obtain an observation-based estimate of the APE damping timescale of approximately 1.7 years, slightly longer than previous ocean reanalysis-based estimates. Furthermore, SSHI serves as an indicator for El Niño "flavors" while recording the relative strength of the thermocline feedback. SSHI captures a decadal shift in El Niño–Southern Oscillation properties in early 2000s, with a more tilted mean thermocline and weaker thermocline slope variations indicative of the "Central Pacific" El Niño type dominating the past two decades, whereas SSH averaged over the tropical Pacific (a proxy for upper-ocean heat content) shows a significant rising trend over this time.

Plain Language Summary El Niño is the warm phase of a climate oscillation originating in the tropical Pacific typically referred to as the El Niño–Southern Oscillation. The maximum sea surface temperature anomaly of canonical El Niño, called Eastern Pacific (EP) El Niño, is located over the equatorial EP. In recent years, another type of El Niño has become more prominent with its maximum sea surface temperature anomaly over the equatorial Central Pacific (CP), termed CP El Niño. Scientists often use variations in the available potential energy (APE) of the tropical ocean to describe El Niño–Southern Oscillation. However, APE computation requires accurate ocean subsurface data. Here, we describe a sea surface height-based index, SSHI, that accurately captures APE changes but can be easily computed from satellite observations. Negative SSHI indicates a flatter thermocline and an El Niño state. We show that larger negative SSHI values typically indicate EP events, while small negative values tend to coincide with CP events. Moreover, SSHI indicates a more tilted mean thermocline and weaker thermocline slope variations after the early 2000s, indicative of the dominant "Central Pacific" El Niño. Using SSHI, we obtain an observation-based estimate of APE damping timescale at approximately 1.7 years.

1. Introduction

The El Niño–Southern Oscillation (ENSO) dominates climate variability in the tropical Pacific (TP) and exerts a strong control on global climate (Clarke, 2008; Philander, 1990; Sarachik & Cane, 2010). Despite substantial progress in understanding and predicting this phenomenon, a number of important issues remain unresolved. In particular, the diversity of El Niño events within a broad ENSO continuum (e.g., Capotondi et al., 2015; Fedorov et al., 2015; Ray & Giese, 2012; Takahashi & Dewitte, 2016) and potential changes in El Niño properties with climate change (e.g., Cai et al., 2014; Fedorov & Philander, 2000; Hu & Fedorov, 2018; Yeh et al., 2009) have attracted intense attention.

Each El Niño event is distinct in terms of its magnitude, spatial structure of sea surface temperature (SST) anomalies, and global teleconnections (see a review by Capotondi et al., 2015). Recent studies distinguish between the conventional El Niño events with the maximum SST anomalies located in the equatorial eastern Pacific (EP) and those with the maximum warming in the equatorial central Pacific (CP), typically referred to as EP El Niño and CP El Niño, respectively (Fedorov et al., 2015; Kao & Yu, 2009). Other terminologies have

been also used, such as the cold tongue El Niño and warm pool El Niño (Kug et al., 2009), or canonical El Niño and El Niño Modoki (Ashok et al., 2007).

It has been argued that CP events may have become more frequent during the first two decades of the 21st century (Lee & McPhaden, 2010; Sullivan et al., 2016; Yeh et al., 2009) and that different flavors of El Niño could have different global climate impacts (e.g., Ding et al., 2011; Gierach et al., 2012; Kim et al., 2009; Yu & Kim, 2011). However, it is still controversial why there have been more CP than EP events recently (e.g., Hu & Fedorov, 2018) and whether CP and EP events are controlled by different dynamical mechanisms (e.g., Kao & Yu, 2009; Kug et al., 2009; Ren & Jin, 2013). Furthermore, whether one can clearly distinguish CP and EP La Niña is hotly debated as some researchers argue that the center of negative SST anomalies does not shift significantly among La Niña events (Kug et al., 2009; Kug & Ham, 2011; Ren & Jin, 2011). Nevertheless, other studies claim that CP La Niña events can be distinguished from the EP type by looking at ocean surface currents (Shinoda et al., 2013) and climate impacts (Cai & Cowan, 2009; Shi & Qian, 2018; Zhang et al., 2015).

In recent years, the ocean energetics framework has been demonstrated to be a useful tool for studying tropical ocean-atmosphere interactions and ENSO (Brown et al., 2011; Brown & Fedorov, 2010; Fedorov, 2002, 2007; Fedorov et al., 2003; Goddard & Philander, 2000; Hu et al., 2014; Kodama & Burls, 2019; Oort et al., 1989; Wunsch, 1998). In the TP, the available potential energy (APE) is a measure of the thermocline slope that reflects the displacement of isopycnals along the equator (e.g., Brown & Fedorov, 2008; Fedorov et al., 2003). The development of El Niño is accompanied by a reduction in wind power that causes a decrease in the APE and a flatter thermocline. In contrast, La Niña is preceded by an increase in wind power that gives rise to an increase in the APE and a more tilted thermocline. Hu et al. (2014) has shown that higher (lower) negative APE values typically correspond to EP (CP) El Niño events.

The rate of change of APE in TP is determined by the power generated by surface winds (wind power in short) minus damping by various oceanic processes, including friction and turbulent diffusion. Following Brown and Fedorov (2010) and Brown et al. (2011), this relationship can be described as

$$\frac{\partial E}{\partial t} = \gamma W - \alpha E \tag{1}$$

In equation 1, anomalous wind power (W) is generated when winds supply (remove) energy to (from) the ocean by acting in the same (opposite) direction as the surface currents. The wind power alters the APE (denoted by E) via buoyancy power, associated with vertical mass fluxes that modify the slope of isopycnals. The two parameters, γ and α, describe integral characteristics of the TP basin: γ is the efficiency of wind power to buoyancy power conversion ($0 < \gamma < 1$) and α is the damping rate of APE (α^{-1} gives the e-folding damping timescale). This damping rate accounts for all different dissipative processes in the tropical basin and is crucial for understanding the lifetime of ENSO cycle. A detailed schematic of energy transfer during ENSO and the role of γ and α are sketched in Figure 1.

However, the difficulty of using ocean energetics resides in the computation of the key variables directly from the observations, which requires accurate, high-resolution data of ocean subsurface density variations in the TP. Such data are currently hard to obtain and the best data come from ocean observations assimilated in general circulation models. While Brown et al. (2011) investigated these parameters using ocean-only models, coupled models, and data assimilation products, it is useful to estimate γ and α directly from the observations. In this study, we will try to circumvent this problem by using sea surface height (SSH) that can be measured from satellites to approximate ocean energetics.

Based on the close relationship between SSH and the ocean thermocline depth, the main objective of this study is to develop an SSH-based index (SSHI) for the APE and to apply it in order to improve our understanding of the diversity and decadal changes of ENSO and to estimate energy dissipation rates in the TP relevant to ENSO.

2. Data and Indices

We calculate the APE and wind power using equations (2) and (3) of Goddard and Philander (2000). For further details, see Brown et al. (2011) and Hu et al. (2014).

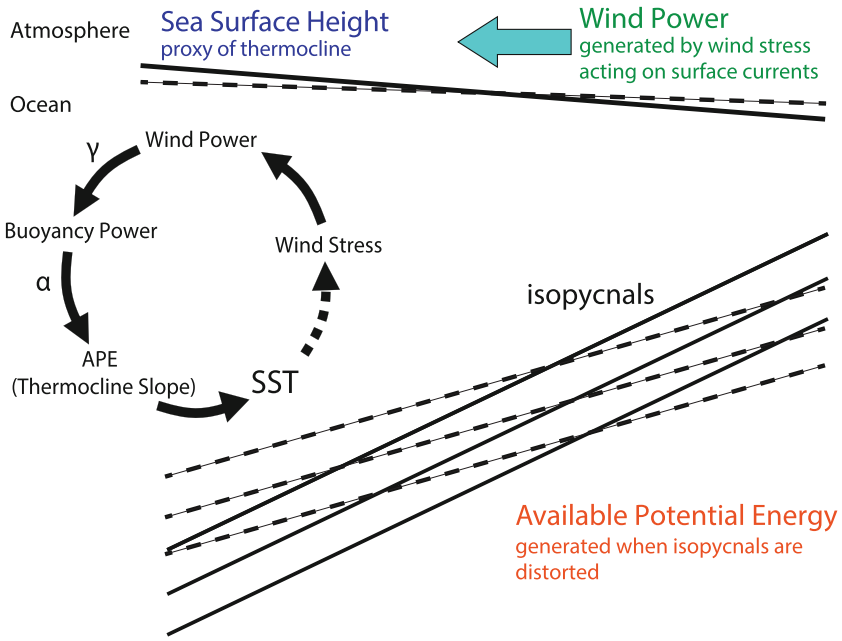

Figure 1. A schematic of the ocean energetics and energy cycle in the tropical basins. Wind power (i.e., the rate of work, in watts) is generated by zonal wind stress acting on surface currents. The vertical displacement of the isopycnals changes the APE of the ocean. Changes in the isopycnal slope affect SST and hence wind stress via ocean-atmosphere coupling. The APE estimated for the TP basin is largely a measure of the thermocline slope along the equator. Sea surface height (SSH) is also a close proxy of the local thermocline depth. Straight dashed lines indicate a flatter air-sea interface and flatter isopycnals. Modified after Brown et al. (2011).

$$E = \iiint \frac{\widetilde{\rho}^2}{2S^2} dV \tag{2}$$

$$W = \iint \vec{u} \cdot \vec{\tau} dA \tag{3}$$

where anomalies of potential density with respect to a reference density profile, given by $\widetilde{\rho} = \rho - \rho^*(z)$, are computed from temperature and salinity using a linearized equation of state for seawater (Goddard & Philander, 2000), where $\rho^*(z)$ is a time-mean horizontal average for potential density over the TP basin. The $S^2 = -(1/g)d\rho^*(z)/dz$ describes ocean vertical stability. We utilize data derived from the Simple Ocean Data Assimilation version 3.4.2 to compute the APE (Carton et al., 2018).

In equation 3, $\vec{\tau} = (\tau_x, \tau_y)$ describes wind stress, for which we use the National Oceanic and Atmospheric Administration (NOAA) National Climatic Data Center blended sea surface winds that combine multiple satellite (DMSP SSMIs, TMI, QuikSCAT, and AMSR-E) observations for wind speed with NCEP Reanalysis 2 for wind direction (Zhang et al., 2006). The wind data set has a horizontal resolution of 0.25° by 0.25° and a daily temporal resolution from 1988 to the present. We compute surface wind stress based on the bulk formula in Harrison and Chiodi (2009). The $\vec{u} = (u, v)$ describes surface currents for which we use the satellite-derived Ocean Surface Current Analyses-Real time current data (Bonjean & Lagerloef, 2002). A indicates the area (15°S to 15°N, 140°E to 80°W), and V denotes the volume of TP basin within 0–400 m as Brown and Fedorov (2010). Typically, the meridional contribution in equation 3 is neglected. Following previous studies (e.g., Goddard & Philander, 2000; Hu et al., 2014), here we focus on the linear components of E and W, that is, $\iiint \frac{\overline{\rho}\rho'}{S^2} dV$ and $\iint \left(\overline{u} \cdot \tau_x' + u' \cdot \overline{\tau}_x\right) dA$, respectively, because the nonlinear APE component does not distinguish between El Niño and La Niña events. In a simple 1.5-layer shallow-water model of the tropical ocean, the thermocline depth anomaly h and SSH anomaly η are related as $\eta = -\frac{\Delta\rho}{\rho} h$, where $\frac{\Delta\rho}{\rho}$ is the relative density jump across the thermocline (Figure 1)

(e.g., Fedorov & Brown, 2009). This is our motivation to introduce SSHI, see equation 4, as an analogue to the APE in this framework (E'; equation 5). Specifically, the SSHI is defined as the product of $\overline{\eta}\eta'$ averaged over a larger TP basin (15°S to 15°N, 120°E to 80°W; denoted by A', which includes more of the warm pool), where $\overline{\eta}$ and η' are the SSH monthly climatology and anomaly, respectively (i.e., $\eta = \overline{\eta} + \eta'$):

$$SSHI = \frac{\iint \overline{\eta}\eta' dA'}{A'} \tag{4}$$

$$E' = \iint g^* \overline{h} h' dA \tag{5}$$

The similarity between equations 4 and 5 implies the potential for SSHI to serve as an index for APE, as we will demonstrate later. Similar to the calculations of E and W, only the linear component of the perturbation is considered here. Note that SSHI is an integral quantity over a zonally larger TP basin than that in equations 2 and 5, which hardly affects the results though ($r = 0.99$).

For the SSH data, we use a multisatellite data set produced by Ssalto/Duacs and distributed by AVISO, with support from the Centre National d'Etudes Spatiales in France. Its main contributors are satellites TOPEX/Poseidon, Jason-1, and Jason-2 from the National Aeronautics and Space Administration, as well as other satellites operated by the European Space Agency and NOAA. The data have a high horizontal resolution of 0.25° by 0.25° globally and a daily temporal resolution spanning the period from 1993 to 2016. The SSH data are sufficient to resolve oceanic Kelvin and Rossby waves critical for the ocean response to intraseasonal wind bursts and the development of El Niño events (e.g., Hu & Fedorov, 2019; Levine & McPhaden, 2016; McPhaden & Yu, 1999).

In addition, the Niño3, Niño4, and Niño3.4 indices are defined as SST anomalies averaged over the equatorial band (5°S to 5°N) within 150–90°W, 160°E–150°W, and 170–120°W, respectively. We use the NOAA Optimum Interpolation SST data (Reynolds et al., 2002). The period for climatology is 1985–2014 for Niño indices but 1994–2016 for other indices, depending on data coverage. The anomalies are estimated as departures from the climatology. The linear trends in the aforementioned indices are all retained.

All the data sets used here bear a certain degree of observational errors. For example, the average errors associated with the NOAA National Climatic Data Center surface zonal wind and the Ocean Surface Current Analyses-Real time surface zonal current are about 0.3 (Peng et al., 2011, 2013) and 0.1 m/s (Johnson et al., 2007), respectively, when evaluated against in situ measurements in equatorial Pacific. But the correlations as we will show later, for example, between W and $dSSHI/dt$ (Figure 5a), suggest that the basic energetics of ENSO system can be well captured by those independent data sets regardless of the existing uncertainties.

3. SSH and El Niño Diversity

The mean thermocline depth and thermocline slope are two key elements that determine the tropical mean state and variability on different timescales (Fedorov & Philander, 2001; Guilyardi et al., 2009; Zelle et al., 2004). The SSHI, which characterizes an average east-west slope of the sea surface, is designed to capture the thermocline tilt, and indeed, it is highly correlated with the linear component of the monthly APE ($r = 0.95$; Figures 2b and 2c). Therefore, SSHI can accurately capture the variations of APE and act as an indicator of ocean energetics. Just as the APE, SSHI is anticorrelated with the monthly Niño3 index ($r = -0.81$; Figures 2a and 2c), implying that the east-west sea level (or thermocline) slope becomes flatter during El Niño events and vice versa during La Niña. The correlation between SSHI and the Niño3.4 index is slightly lower ($r = -0.78$; supporting information Figure S1).

The SSH anomaly averaged over the TP, a proxy of ocean heat content (OHC) of the upper ocean, shows a significant rising trend (Figure 2d), which reflects the changes in the tropical climate associated with global warming (also Figure 2e) and can be partly attributed to the effects of zonal wind strengthening in the TP since the 1990s (e.g., England et al., 2014; Merrifield, 2011; Takahashi & Watanabe, 2016; Zhao & Fedorov, 2019). These mean wind changes have been accompanied by more frequent CP events (Choi et al., 2011; Chung & Li, 2013; Xiang et al., 2013). Stronger winds keep a large amount of warm water

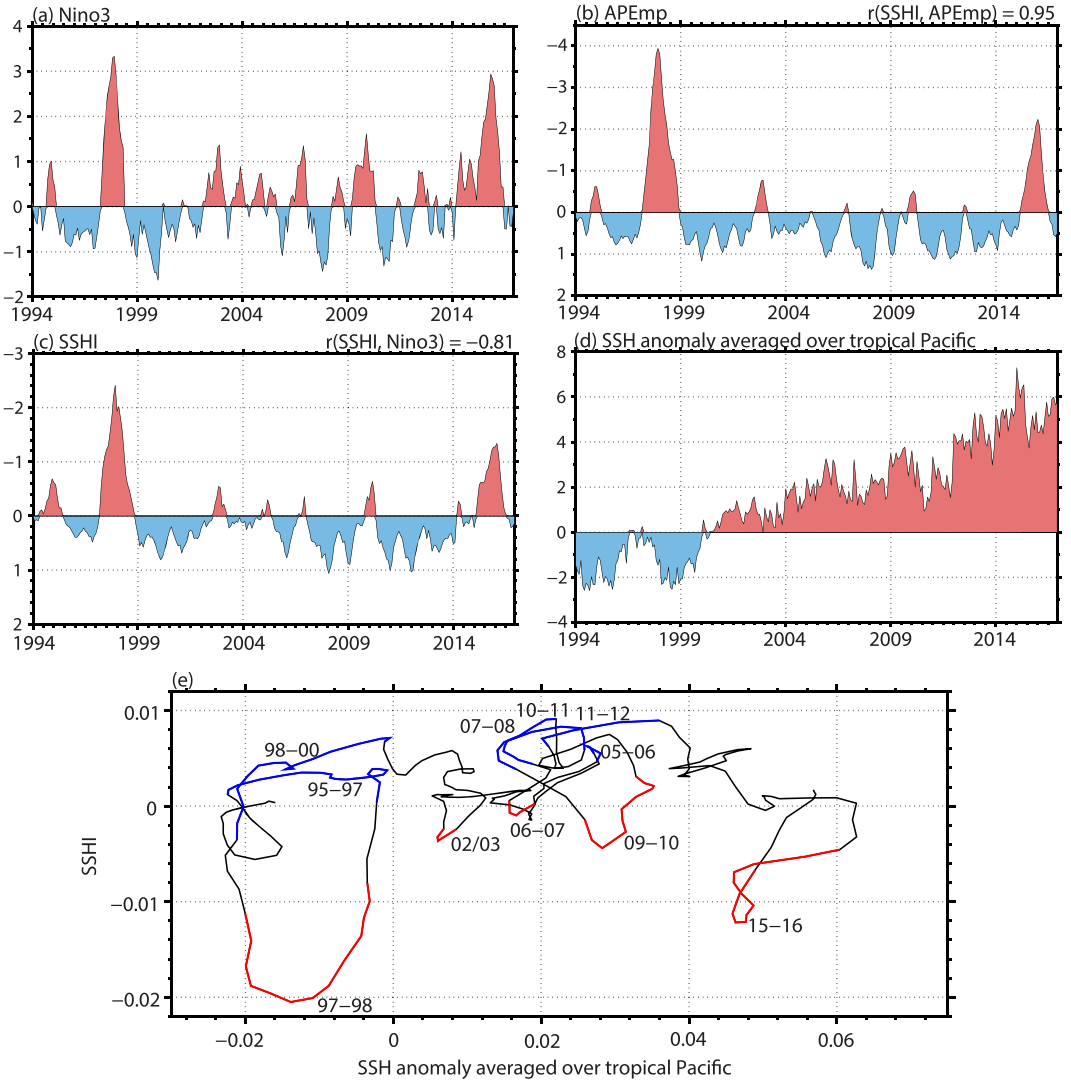

Figure 2. Monthly variations of (a) the Niño3 index, (b) the linear component of APE (APE_{mp}, units: 10^{18} J) derived from equation 2, (c) the SSH index (SSHI, units: 10^{-2} m^2), and (d) mean SSH anomaly (units: 10^{-2} m) averaged in the TP basin (15°S to 15°N, 120°E to 80°W) from 1994 to 2016. The SSHI in (c) is computed following equation 4 and is a measure of the thermocline slope. Correlation coefficients *r* are shown at the top right corner of panels (b) and (c). The vertical axis is reversed in panels (b) and (c) for better comparison with the Niño3 index. (e) The system's trajectory showing SSHI (from panel c) versus SSH anomaly averaged over the TP (from panel d) with a 5 month running mean applied. El Niño (La Niña) events are marked as red (blue) parts of the trajectory with the Niño-3 index larger (smaller) than 0.5 °C (−0.5 °C) for at least 5 months with at most 1 month interruption. Note the gradual drift of the system toward positive values of average SSH anomaly (from left to right), indicative of OHC increase, and much weaker SSHI negative excursions after 1997/1998, indicative of the shift to CP El Niño events.

locked in the western TP. This persistent trend, as seen in SSH, appears to be not as prominent in other OHC indices, such as warm water volume and T300 (mean ocean temperature anomaly in the upper 300 m) when averaged between 15°S and 15°N, possibly due to additional factors such as salinity variations that can affect SSH but not temperature-based indices.

The contribution of western TP to the overall SSH rising trend was documented in Merrifield (2011) who compared satellite altimetry with direct observations of tide gauges. This author also argued that interannual sea level variations associated with ENSO events did not account for this trend. Nor did this trend show the global warming hiatus between years 2000 and 2013 evident in global mean surface temperature (e.g., Fyfe et al., 2016; Hu & Fedorov, 2017; Kosaka & Xie, 2013; Schmidt et al., 2014).

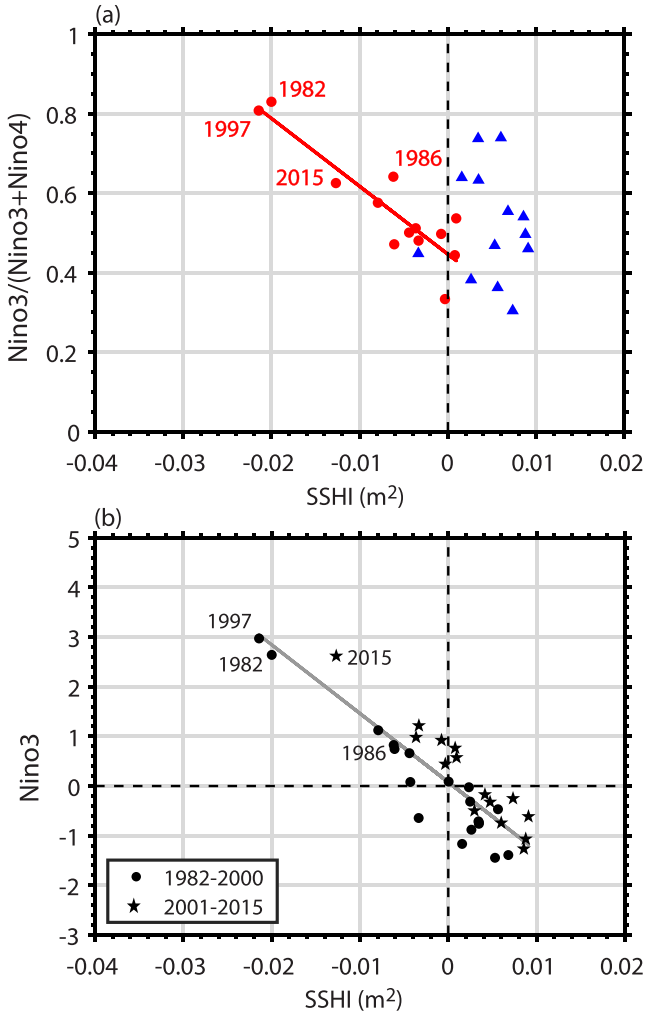

Figure 3. (a) The ratio of the Niño3 index to the sum Niño3 + Niño4 versus SSHI between 1982 and 2015 with all variables estimated for boreal winter (average for November-December-January-February). The SSHI data for the period 1982–1993 are derived from a linear regression of SSHI against APE_{mp}. Years with positive (negative) Niño3 and Niño4 indices greater than 0.5 °C (smaller than −0.5 °C) are marked as red dots (blue triangles) for warm (cold) events. The red line gives the best linear fit for El Niño events (regression would not be significant for La Niña events). (b) As in panel (a) but with the Niño3 index shown on the y axis. To highlight the decadal change of SSHI, results before and after the year 2000 are marked as dots and pentagrams, respectively. The gray line gives the best linear fit for the whole period. Dashed vertical and horizontal lines denote zero. Four EP El Niño events are annotated.

Next, we will show how SSHI could be used to distinguish between EP and CP El Niño events. To characterize the El Niño type we use a simple index Niño3/(Niño3 + Niño4) with larger values indicating more EP-like events. We find a linear correlation between the winter-mean index for El Niño type and SSHI ($r = -0.90$; Figure 3a). Larger (smaller) negative SSHI values correspond to EP (CP) El Niño (Figure 3a), consistent with Hu et al. (2014) that used the APE and found a similar relationship. Thermocline variations and the associated thermocline feedback are more effective in EP El Niño than CP El Niño; see for example, Kug et al. (2009) or Fedorov et al. (2015). The correlation would be 0.84 if Niño3 itself were used as an indicator of El Niño type (in line with the notion that EP El Niño events are typically more intense than the CP events). In contrast, the connection between SSHI and event type becomes looser for La Niña events (Figure 3a), suggesting that thermocline variations may be less important in determining La Niña type. This is confirmed by a composite analysis following the event classification of Shi and Qian (2018), which shows that the pattern and magnitude of SSH anomalies demonstrate greater differences between the two El Niño types than those between the two La Niña types (Figures 4 and S2).

The described differences in thermocline variability between CP and EP El Niño are consistent with previous theoretical, modeling, and observational studies (e.g., Hu & Fedorov, 2019; Kug et al., 2009; Xie & Jin, 2018). Moreover, the observed small difference between CP and EP La Niña is not inconsistent with the previous work that did not find significant differences in La Niña flavors (e.g., Kug & Ham, 2011; Ren & Jin, 2011).

Figure 3b confirms the close linear relationship between Niño3 and SSHI on interannual timescales. On longer timescales, the basin-integrated SSHI has experienced a more pronounced decadal shift in El Niño properties as compared to the Niño3 index (Figures 2c and 3b), which is also evident in other CP indices (Sullivan et al., 2016).

4. SSHI-Based Estimate of Energy Damping Rate

Further, to estimate net energy dissipation rate in the TP, we employ SSHI as an observation-based proxy of the APE and arrive at equation 6.

$$\frac{dSSHI}{dt} = \gamma' W - \alpha' SSHI \tag{6}$$

Here, γ' is a dimensional coefficient calculated by the least squares fit between the first two terms that indicates the efficiency from wind power to SSHI. For seasonal-mean results, the rate of change of SSHI has a high correlation ($r = 0.84$) with wind power anomalies (Figure 5a), which indicates that the wind power indeed controls thermocline changes and the influence of observational errors associated with zonal wind and current on W is relatively small. The correlation coefficient here is a little lower than correlations calculated from the ocean-only models and data assimilations (Brown & Fedorov, 2010), which may result from stronger noise contained in the observational data sets. Brown et al. (2011) documented that the majority of the coupled models showed a relatively low efficiency (values of γ in the range of 10–50% versus 50–60% for ocean-only simulations or ocean reanalysis). Here, we would be able to estimate such efficiency based on SSHI only if we converted SSHI to the APE with the aid of ocean reanalysis. In other words, the parameter γ' estimated using

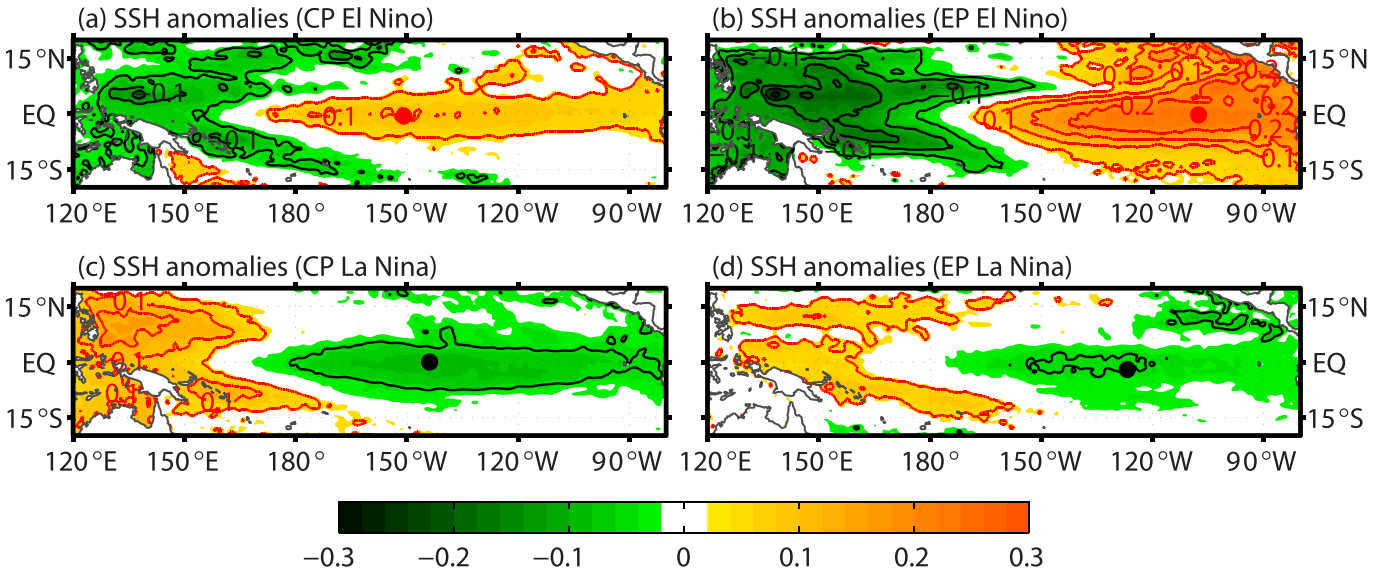

Figure 4. Composites of winter-mean SSH anomalies (color shading with contours, in meters; 0.05 m contour interval) for different event types after the year 1994: (a) CP El Niño (1994 and 2009), (b) EP El Niño (1997 and 2015), (c) CP La Niña (1998, 2000, 2008, and 2011), and (d) EP La Niña (1995 and 2005). Red (black) dots indicate the centers of maximum (minimum) anomalous SSH. No significance test is shown here due to the small sample size.

SSHI and W is not a dimensionless variable and cannot be directly compared with γ estimated by previous studies.

However, we are able to estimate the physically meaningful parameter α' (i.e., energy dissipation rate) purely based on SSHI and W. In particular, we can compute α' by regressing the residual part of SSHI tendency after subtracting the wind power component (i.e., $\frac{dSSHI}{dt} - \gamma' W$) to SSHI. Various processes contribute to the energy dissipation, such as turbulent diffusion, generation of equatorial Kelvin and Rossby waves, generation of tropical instability waves, energy advection out of the Pacific basin, and damping by surface heat fluxes. All these processes can be incorporated into a linear damping term and the α'^{-1} gives the damping timescale of SSHI. We estimate the damping timescale as 1.7 ± 0.5 years at 95% confidence level (Figure 5b). Again, the two energy metrics γ' and α' incorporate subsurface TP dynamics and hence provide a basin-wide averaged, physical measure of the dissipation.

We have repeated the aforementioned analysis using monthly data and get similar results with slightly lower correlations (Figures 5c and 5d). The damping timescale using monthly data is 1.4 ± 0.3 years at 95% confidence level. For comparison, the damping timescale falls within 0.4–1 year for coupled models and 0.9–1.2 years for ocean-only simulations and ocean reanalysis (Brown et al., 2011), which is shorter than that of the observational-based results here. Repeating the analysis using the APE rather than SSHI yields slightly lower correlations and a damping timescale in the [1.5, 4.5] year range (Figures 5e and 5f). This timescale is somewhat longer than the ocean reanalysis-based results in Brown et al. (2011), possibly due to different periods, lengths, and sources of the data. Comparing all these data suggests that 1 to 2 years damping timescale arising from our SSHI analysis is a reasonable estimate, but longer data are needed to constrain this value better.

It should be emphasized that the above results are based on the linearized part of the APE (or SSHI) and wind power anomalies because the linear terms dominate. Incorporating the nonlinear terms adds noise to the system and degrades the correlations somewhat. Quantitatively, the correlation between the residual and SSHI is only −0.37 after adding nonlinear terms, much lower compared to −0.57 in Figure 5b. Furthermore, it should be noted that the extreme 1997/1998 EP El Niño event significantly contributes to the slope in Figure 5b ($r = -0.39$ after removing the dots during the 1997/1998 event), while La Niña events appear to matter much less. This asymmetry might potentially indicate different damping rates between warm and cold ENSO phases. Although the slope from our current analysis is statistically significant (Figure 5), longer data sets will be needed to clarify this issue.

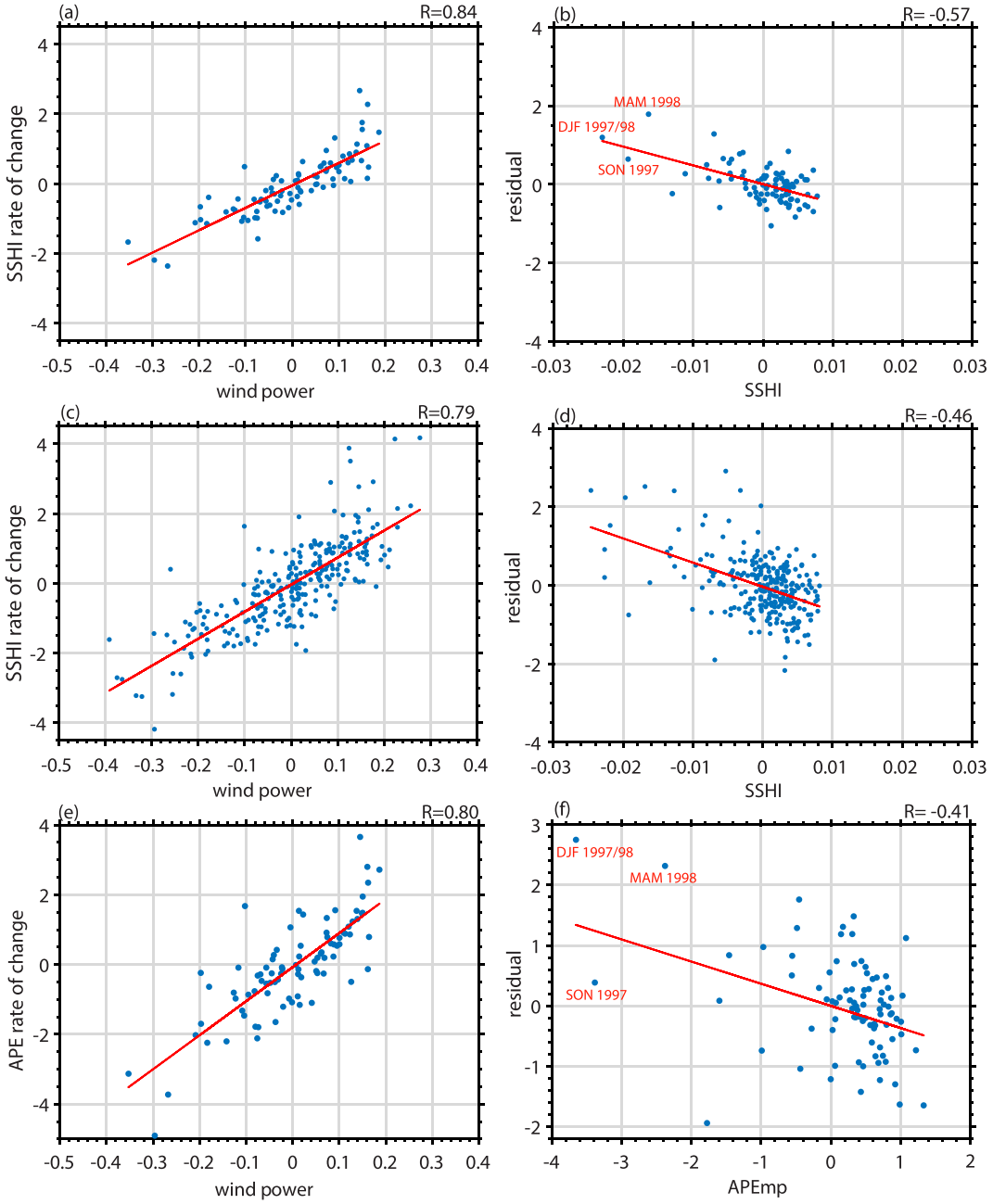

Figure 5. Scatterplots of (a) the seasonal-mean SSHI rate of change (units: 10^{-3} m^2 per month) versus wind power anomalies (units: terawatts) and (b) the corresponding residual (computed as $\frac{dSSHI}{dt} - \gamma' W$; units: 10^{-3} m^2 per month) versus SSHI anomalies (units: m^2). Red lines indicate the least squares fit. Regressing the residual onto SSHI gives a damping timescale for SSHI of approximately 1.7 ± 0.5 years at a 95% confidence level. Correlation coefficients R are shown at the top right corner of each panel. Seasonal-mean values are calculated by averaging March-April-May values for spring, June-July-August values for summer, September-October-November values for autumn, and December-January-February values for winter. (c, d) As in panels (a) and (b) but for monthly data with the damping timescale estimated as 1.4 ± 0.3 years at a 95% confidence level. Also shown are scatterplots of (e) seasonal-mean APE_{mp} rate of change (units: 10^{17} J per month) versus wind power anomalies and (f) the corresponding residual ($\frac{dAPE_{mp}}{dt} - \gamma W$; units: 10^{17} J per month) versus APE_{mp} anomalies (units: 10^{18} J). The damping timescale of APE_{mp} is estimated between [1.5, 4.5] years at a 95% confidence level.

5. Conclusions and Discussion

Ocean energetics framework is a useful diagnostic tool for ENSO cycle (e.g., Brown & Fedorov, 2010; Fedorov et al., 2003; Goddard & Philander, 2000; Hu et al., 2014). In this perspective, the APE is an integral measure that provides information on thermocline variations over the TP basin forced by changes in surface wind stress. In this study we have proposed a new index, SSHI, that can serve as a proxy for the linearized APE with a correlation coefficient of 0.95, indicating the high ability of SSHI to represent the ocean energetics. The SSHI and the Niño3 index are anticorrelated, but they reveal complementary characteristics of the coupled system over TP. For example, SSHI can be used to distinguish El Niño types with a larger (smaller) negative value corresponding to EP (CP) El Niño. However, the linkage between SSHI and event type becomes much looser for La Niña. On the other hand, the mean SSH anomaly over TP, indicating the OHC below, demonstrates a significant rising trend consistent with global warming.

We show that the *e*-folding damping timescale of SSHI is estimated within approximately 1.4 ± 0.3 years when based on monthly data and 1.7 ± 0.5 years when based on seasonal data. This damping timescale is a little longer than 0.9–1.2 years obtained by Brown et al. (2011) from ocean reanalysis, but, given the results' error bars, they are not inconsistent. Several potential reasons could be responsible for this difference, including (1) too strong damping processes and parameterizations (e.g., excessive diffusive dissipation) incorporated in ocean-only, data-assimilating, and coupled models and (2) model biases in the wind field, ocean thermal structure and currents. Regardless of these issues, this damping timescale, associated with the large-scale oceanic motion, largely influences the system's stability and other relevant properties. Therefore, the metric α' indicating the energy dissipation in the tropical ocean can be applied to both ocean-only and coupled models for their intercomparison and evaluation.

Acknowledgments
This research is supported by grants to A. V. F. from NASA (NNX17AH21G) and NSF (AGS-0163807). J. S. acknowledges the funding from the National Natural Science Foundation of China (41775067), the Fundamental Research Funds for the Central Universities (842013033), and the China Scholarship Council (CSC). S. H. is supported by the Scripps Institutional Postdoctoral Fellowship and the Lamont-Doherty Postdoctoral Fellowship. The SSH data are available at the website (https://www.aviso.altimetry.fr/en/data/products/sea--surface-height-products/global.html). The surface wind data can be found online (https://www.ncdc.noaa.gov/data-access/marineocean-data/blended-global/blended-sea-winds). The OSCAR current data can be found online (https://podaac.jpl.nasa.gov/dataset/OSCAR_L4_OC_third-deg). The OISST and SODA data are available online (at https://www.ncdc.noaa.gov/oisst and http://www.soda.umd.edu/, respectively).

References

Ashok, K., Behera, S. K., Rao, S. A., Weng, H., & Yamagata, T. (2007). El Niño Modoki and its possible teleconnection. *Journal of Geophysical Research*, *112*, C11007. https://doi.org/10.1029/2006JC003798

Bonjean, F., & Lagerloef, G. S. (2002). Diagnostic model and analysis of the surface currents in the tropical Pacific Ocean. *Journal of Physical Oceanography*, *32*(10), 2938–2954.

Brown, J. N., & Fedorov, A. V. (2008). Mean energy balance in the tropical Pacific Ocean. *Journal of Marine Research*, *66*, 1–23.

Brown, J. N., & Fedorov, A. V. (2010). How much energy is transferred from the winds to the thermocline on ENSO timescales? *Journal of Climate*, *23*, 1563–1580.

Brown, J. N., Fedorov, A. V., & Guilyardi, E. (2011). How well do coupled models replicate ocean energetics relevant to ENSO? *Climate Dynamics*, *36*(11–12), 2147–2158.

Cai, W., Borlace, S., Lengaigne, M., van Rensch, P., Collins, M., Vecchi, G., et al. (2014). Increasing frequency of extreme El Niño events due to greenhouse warming. *Nature Climate Change*, *4*(2), 111–116. https://doi.org/10.1038/nclimate2100

Cai, W., & Cowan, T. (2009). La Niña Modoki impacts Australia autumn rainfall variability. *Geophysical Research Letters*, *36*, L12805. https://doi.org/10.1029/2009GL037885

Capotondi, A., Wittenberg, A. T., Newman, M., di Lorenzo, E., Yu, J. Y., Braconnot, P., et al. (2015). Understanding ENSO diversity. *Bulletin of the American Meteorological Society*, *96*(6), 921–938. https://doi.org/10.1175/BAMS-D-13-00117.1

Carton, J. A., Chepurin, G. A., & Chen, L. (2018). SODA3: A new ocean climate reanalysis. *Journal of Climate*, *31*, 6967–6983.

Choi, J., An, S. I., Kug, J. S., & Yeh, S. W. (2011). The role of mean state on changes in El Niño's flavor. *Climate Dynamics*, *37*, 1205–1215.

Chung, P. H., & Li, T. (2013). Interdecadal relationship between the mean state and El Niño types. *Journal of Climate*, *26*, 361–379.

Clarke, A. J. (2008). *An introduction to the dynamics of El Niño & the Southern Oscillation*. London: Academic Press.

Ding, Q. H., Steig, E. J., Battisti, D. S., & Kuttel, M. (2011). Winter warming in West Antarctica caused by central tropical Pacific warming. *Nature Geoscience*, *4*(6), 398–403. https://doi.org/10.1038/Ngeo1129

England, M. H., McGregor, S., Spence, P., Meehl, G. A., Timmermann, A., Cai, W., et al. (2014). Recent intensification of wind-driven circulation in the Pacific and the ongoing warming hiatus. *Nature Climate Change*, *4*(3), 222–227.

Fedorov, A. V. (2002). The response of the coupled tropical ocean–atmosphere to westerly wind bursts. *Quarterly Journal of the Royal Meteorological Society*, *128*, 1–23.

Fedorov, A. V. (2007). Net energy dissipation rates in the tropical ocean and ENSO dynamics. *Journal of Climate*, *20*, 1108–1117.

Fedorov, A. V., & Brown, J. N. (2009). Equatorial waves. In J. Steele (Ed.), *Encyclopedia of ocean sciences*. (pp. 3679–3695), (2nd ed.). Dublin: Academic Press.

Fedorov, A. V., Harper, S. L., Philander, S. G., Winter, B., & Wittenberg, A. (2003). How predictable is El Niño? *Bulletin of the American Meteorological Society*, *84*, 911–919.

Fedorov, A. V., Hu, S., Lengaigne, M., & Guilyardi, E. (2015). The impact of westerly wind bursts and ocean initial state on the development, and diversity of El Niño events. *Climate Dynamics*, *44*(5–6), 1381–1401.

Fedorov, A. V., & Philander, S. G. (2000). Is El Niño changing? *Science*, *288*(5473), 1997–2002. https://doi.org/10.1126/Science.288.5473.1997

Fedorov, A. V., & Philander, S. G. (2001). A stability analysis of tropical ocean–atmosphere interactions: Bridging measurements and theory for El Niño. *Journal of Climate*, *14*(14), 3086–3101.

Fyfe, J. C., Meehl, G. A., England, M. H., Mann, M. E., Santer, B. D., Flato, G. M., et al. (2016). Making sense of the early-2000s warming slowdown. *Nature Climate Change*, *6*(3), 224–228. https://doi.org/10.1038/nclimate2938

Gierach, M. M., Lee, T., Turk, D., & McPhaden, M. J. (2012). Biological response to the 1997–98 and 2009–10 El Niño events in the equatorial Pacific Ocean. *Geophysical Research Letters*, *39*, L10602. https://doi.org/10.1029/2012GL051103
Goddard, L., & Philander, S. G. H. (2000). The energetics of El Niño and La Niña. *Journal of Climate*, *13*, 1496–1516.
Guilyardi, E., Wittenberg, A., Fedorov, A., Collins, M., Wang, C., Capotondi, A., et al. (2009). Understanding El Niño in ocean–atmosphere general circulation models: Progress and challenges. *Bulletin of the American Meteorological Society*, *90*(3), 325–340.
Harrison, D. E., & Chiodi, A. M. (2009). Pre-and post-1997/98 westerly wind events and equatorial Pacific cold tongue warming. *Journal of Climate*, *22*(3), 568–581.
Hu, S., & Fedorov, A. V. (2017). The extreme El Niño of 2015–2016 and the end of global warming hiatus. *Geophysical Research Letters*, *44*, 3816–3824. https://doi.org/10.1002/2017GL072908
Hu, S., & Fedorov, A. V. (2018). Cross-equatorial winds control El Niño diversity and change. *Nature Climate Change*, *8*(9), 798–802.
Hu, S., & Fedorov, A. V. (2019). The extreme El Niño of 2015–2016: The role of westerly and easterly wind bursts, and preconditioning by the failed 2014 event. *Climate Dynamics*, *52*(12), 7339–7357.
Hu, S., Fedorov, A. V., Lengaigne, M., & Guilyardi, E. (2014). The impact of westerly wind bursts on the diversity and predictability of El Niño events: An ocean energetics perspective. *Geophysical Research Letters*, *41*, 4654–4663. https://doi.org/10.1002/2014GL059573
Johnson, E. S., Bonjean, F., Lagerloef, G. S., Gunn, J. T., & Mitchum, G. T. (2007). Validation and error analysis of OSCAR Sea surface currents. *Journal of Atmospheric and Oceanic Technology*, *24*(4), 688–701.
Kao, H. Y., & Yu, J. Y. (2009). Contrasting Eastern-Pacific and Central-Pacific types of ENSO. *Journal of Climate*, *22*(3), 615–632.
Kim, H. M., Webster, P. J., & Curry, J. A. (2009). Impact of shifting patterns of Pacific Ocean warming on North Atlantic tropical cyclones. *Science*, *325*(5936), 77–80. https://doi.org/10.1126/Science.1174062
Kodama, K., & Burls, N. J. (2019). An empirical adjusted ENSO ocean energetics framework based on observational wind power in the tropical Pacific. *Climate Dynamics*, *53*(5–6), 3271–3288.
Kosaka, Y., & Xie, S. P. (2013). Recent global-warming hiatus tied to equatorial Pacific surface cooling. *Nature*, *501*(7467), 403–407. https://doi.org/10.1038/nature12534
Kug, J. S., & Ham, Y. G. (2011). Are there two types of La Nina? *Geophysical Research Letters*, *38*, L16704. https://doi.org/10.1029/2011GL048237
Kug, J. S., Jin, F. F., & An, S. I. (2009). Two types of El Niño events: Cold tongue El Niño and warm Pool El Niño. *Journal of Climate*, *22*(6), 1499–1515.
Lee, T., & McPhaden, M. J. (2010). Increasing intensity of El Niño in the central-equatorial Pacific. *Geophysical Research Letters*, *37*, L14603. https://doi.org/10.1029/2010GL044007
Levine, A. F., & McPhaden, M. J. (2016). How the July 2014 easterly wind burst gave the 2015–2016 El Niño a head start. *Geophysical Research Letters*, *43*, 6503–6510. https://doi.org/10.1002/2016GL069204
McPhaden, M. J., & Yu, X. (1999). Equatorial waves and the 1997–98 El Niño. *Geophysical Research Letters*, *26*(19), 2961–2964. https://doi.org/10.1029/1999GL004901
Merrifield, M. A. (2011). A shift in western tropical Pacific Sea level trends during the 1990s. *Journal of Climate*, *24*(15), 4126–4138.
Oort, A. H., Ascher, S. C., Levitus, S., & Peixoto, J. P. (1989). New estimates of the available potential energy in the world ocean. *Journal of Geophysical Research*, *94*, 3187–3200.
Peng, G., Zhang, H. M., Frank, H. P., Bidlot, J. R., Higaki, M., & Hankins, W. (2011). A comparison of various equatorial pacific surface wind products. In 2011 IEEE International Geoscience and Remote Sensing Symposium (pp. 2049–2052), IEEE.
Peng, G., Zhang, H. M., Frank, H. P., Bidlot, J. R., Higaki, M., Stevens, S., & Hankins, W. R. (2013). Evaluation of various surface wind products with OceanSITES buoy measurements. *Weather and Forecasting*, *28*(6), 1281–1303.
Philander, S. G. (1990). *El Niño, La Niña and the Southern Oscillation*. New York: Academic Press.
Ray, S., & Giese, B. S. (2012). Historical changes in El Niño and La Niña characteristics in an ocean reanalysis. *Journal of Geophysical Research*, *117*, C11007. https://doi.org/10.1029/2012JC008031
Ren, H. L., & Jin, F. F. (2011). Niño indices for two types of ENSO. *Geophysical Research Letters*, *38*, L04704. https://doi.org/10.1029/2010GL046031
Ren, H. L., & Jin, F. F. (2013). Recharge oscillator mechanisms in two types of ENSO. *Journal of Climate*, *26*(17), 6506–6523.
Reynolds, R. W., Rayner, N. A., Smith, T. M., Stokes, D. C., & Wang, W. (2002). An improved in situ and satellite SST analysis for climate. *Journal of Climate*, *15*(13), 1609–1625.
Sarachik, E. S., & Cane, M. A. (2010). *The El Niño-Southern Oscillation phenomenon*. (Vol. 13, p. 369). Cambridge, UK and New York: Cambridge University Press.
Schmidt, G. A., Shindell, D. T., & Tsigaridis, K. (2014). Reconciling warming trends. *Nature Geoscience*, *7*(3), 158–160.
Shi, J., & Qian, W. H. (2018). Asymmetry of two types of ENSO in the transition between the East Asian winter monsoon and the ensuing summer monsoon. *Climate Dynamics*, *51*(9–10), 3907–3926.
Shinoda, T., Hurlburt, H. E., & Metzger, E. J. (2013). Anomalous tropical ocean circulation associated with La Niña Modoki. *Journal of Geophysical Research*, *116*, C12001. https://doi.org/10.1029/2011JC007304
Sullivan, A., Luo, J. J., Hirst, A. C., Bi, D., Cai, W., & He, J. (2016). Robust contribution of decadal anomalies to the frequency of central-Pacific El Niño. *Scientific Reports*, *6*, 38,540.
Takahashi, C., & Watanabe, M. (2016). Pacific trade winds accelerated by aerosol forcing over the past two decades. *Nature Climate Change*, *6*(8), 768–772.
Takahashi, K., & Dewitte, B. (2016). Strong and moderate nonlinear El Niño regimes. *Climate Dynamics*, *46*(5–6), 1627–1645.
Wunsch, C. (1998). The work done by the wind on the oceanic general circulation. *Journal of Physical Oceanography*, *28*, 2332–2340.
Xiang, B., Wang, B., & Li, T. (2013). A new paradigm for the predominance of standing central Pacific warming after the late 1990s. *Climate Dynamics*, *41*, 327–340.
Xie, R., & Jin, F. F. (2018). Two leading ENSO modes and El Niño types in the Zebiak–Cane model. *Journal of Climate*, *31*(5), 1943–1962.
Yeh, S. W., Kug, J. S., Dewitte, B., Kwon, M. H., Kirtman, B. P., & Jin, F. F. (2009). El Niño in a changing climate. *Nature*, *461*(7263), 511–514. https://doi.org/10.1038/Nature08316
Yu, J. Y., & Kim, S. T. (2011). Relationships between extratropical sea level pressure variations and the Central Pacific and Eastern Pacific types of ENSO. *Journal of Climate*, *24*(3), 708–720. https://doi.org/10.1175/2010jcli3688.1
Zelle, H., Appeldoorn, G., Burgers, G., & Van Oldenborgh, G. J. (2004). The relationship between sea surface temperature and thermocline depth in the eastern equatorial Pacific. *Journal of Physical Oceanography*, *34*(3), 643–655.
Zhang, H. M., Bates, J. J., & Reynolds, R. W. (2006). Assessment of composite global sampling: Sea surface wind speed. *Geophysical Research Letters*, *33*, L17714. https://doi.org/10.1029/2006GL027086

Zhang, W. J., Wang, L., Xiang, B. Q., Qi, L., & He, J. H. (2015). Impacts of two types of La Niña on the NAO during boreal winter. *Climate Dynamics*, *44*, 1351–1366.

Zhao, B., & Fedorov, A. V. (2019). The effects of background zonal and meridional winds on ENSO in a coupled GCM. *Journal of Climate*. https://doi.org/10.1175/JCLI-D-18-0822.1